Real-Time Imaging Using a 4.3-THz Quantum Cascade Laser and a 320 × 240 Microbolometer Focal-Plane Array

Alan W. M. Lee, *Student Member, IEEE*, Benjamin S. Williams, *Member, IEEE*, Sushil Kumar, Qing Hu, *Senior Member, IEEE*, and John L. Reno

***Abstract*—We report the use of a ∼50-mW peak power 4.3-THz quantum cascade laser (QCL) as an illumination source for real-time imaging with a 320 × 240 element room-temperature microbolometer focal-plane array detector. The QCL is modulated synchronously with the focal-plane array for differential imaging. Signal-to-noise ratios of ∼340 are achieved at a 20-frame/s acquisition rate, and the optical noise equivalent power of the detector array at 4.3 THz is estimated to be ∼ 320 pW/$\sqrt{\text{Hz}}$. Both reflection and transmission mode imaging are demonstrated.**

***Index Terms*—Imaging, quantum cascade laser (QCL), real time, terahertz.**

TERAHERTZ (THz) frequency range radiation, 0.3–10 THz, has shown promise for security and biomedical imaging applications because of spectral absorption features that allow the measurement of skin hydration for cancer detection, DNA binding state for label-free analysis, or unique absorption peaks in illicit drugs for mail screening [1]–[3]. For these applications, real-time (∼30 frames per second) imaging will be highly desirable, requiring the use of detector arrays and a multifrequency high-power source. The THz quantum cascade laser (QCL) [4]–[6] has demonstrated high peak powers up to ∼250 mW [7], with spectral coverage from 1.9–5.0 THz [7], [8], while also being dimensionally compact, allowing several QCLs of different frequencies to be packaged in an array for multicolor imaging. Imaging with QCLs has been limited to single-element detectors resulting in acquisition times of several minutes [9]. Previously, we demonstrated real-time imaging with a ∼10-mW far-infrared (FIR) gas laser and a 160 × 120 microbolometer focal-plane array [10]. However, the FIR laser is bulky compared to the QCL and has only discrete spectral coverage, precluding its use as a multifrequency source.

Manuscript received February 7, 2006; revised April 6, 2006. This work was supported in part by the Air Force Office of Scientific Research, by the National Aeronautics and Space Administration, and by the National Science Foundation. Sandia is a multiprogram laboratory operated by Sandia Corporation, a Lockheed Martin Company, for the United States Department of Energy's National Nuclear Security Administration under Contract DE-AC04-94AL85000.

A. W. M. Lee, B. S. Williams, S. Kumar, and Q. Hu are with the Department of Electrical Engineering and Computer Science and Research Laboratory of Electronics, Massachusetts Institute of Technology, Cambridge, MA 02139 USA (e-mail: awmlee@mit.edu).

J. L. Reno is with Sandia National Laboratories, Albuquerque, NM 87185-0601 USA.

Digital Object Identifier 10.1109/LPT.2006.877220

In this letter, we demonstrate the use of a 4.3-THz 50-mW QCL source for real-time imaging with a 320 × 240 element microbolometer focal-plane array detector. The QCL is cooled to ∼33 K by a closed-cycle pulse-tube cryorefrigerator (PT60, Cryomech) and is modulated synchronously with the focal-plane array for differential detection. The differential scheme reduces 1/f noise and removes the infrared background, obviating the need for long-wavelength-pass filters. A signal-to-noise (SNR) ratio of ∼340 and an optical noise equivalent power (NEP_O) of 320 pW/$\sqrt{\text{Hz}}$ are measured.

The growth, fabrication, and characterization of the QCL used in this letter are detailed in [7]. Briefly, the laser was grown by molecular beam epitaxy based on the resonant-phonon depopulation scheme [11] and processed into a 98 μm × 2.15 mm semi-insulating surface-plasmon ridge waveguide with the rear facet high-reflectivity coated. This device produces a maximum CW power of 125 mW at 10 K, and when operated at ∼33 K in the cryorefrigerator at 25% duty cycle, the peak power is reduced to 50 mW. At the time of writing, the same device has been operated for over 100 h and 25 thermal cycles with no signs of degradation. The 4.3-THz frequency is conveniently centered in an atmospheric transmission window, which is calculated to have a loss of ∼0.5 dB/m at 25% relative humidity.

The detector is a commercial 320 × 240 pixel, uncooled, vanadium oxide (VO_x) microbolometer focal-plane array camera (SCC500, BAE Systems, Lexington, MA) [12]. Designed for the 7.5–14-μm night vision band, the elements remain absorptive due to the broadband absorbing silicon nitride and VO_x materials used. The microbolometers are spaced at a 46.25-μm pitch and have an electrical noise equivalent power (NEP_E) of 0.9 pW/$\sqrt{\text{Hz}}$ [12].

The imaging setup is shown in Fig. 1. The laser is indium soldered to a copper carrier, which is mounted in the cryorefrigerator. Due to the high angular divergence of the emitted beam the device is placed as close as possible to the polypropylene cryorefrigerator window. An f/1 50-mm diameter off-axis parabolic (OAP) mirror collimates the emerging beam, which is refocused by a second OAP (f/2), back-illuminating an object (an envelope in Fig. 1). Roughly 85% of the light at the window reaches the object, limited by the angle subtended by the first OAP. The transmitted light is imaged by an f/1 25-mm diameter Si meniscus lens, through a Ge vacuum window onto the focal-plane array. A meniscus lens was chosen to minimize the center thickness, reducing the associated absorption losses. The transmission through the lens and window was improved

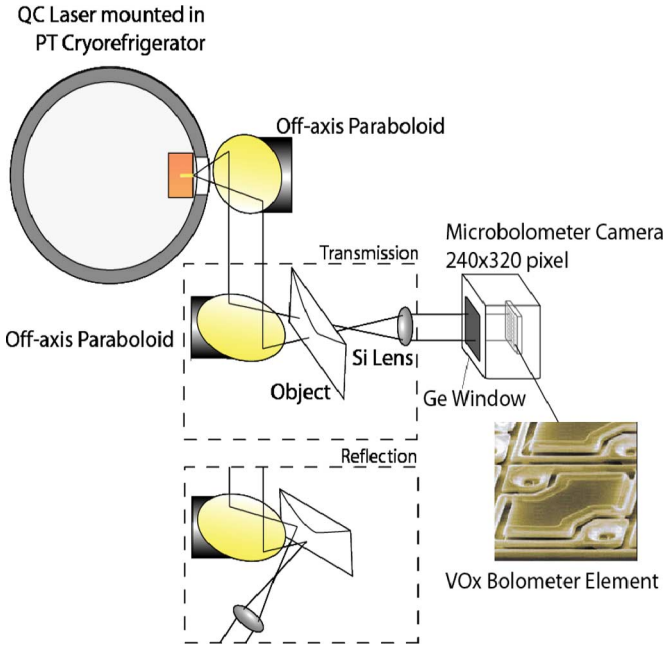

Fig. 1. Experimental setup of terahertz imaging system. Photo shows vanadium oxide microbolometer (courtesy of BAE systems, Lexington, MA). Cutaway depicts alternate reflection mode setup. (Color version available online at http://ieeexplore.ieee.org.)

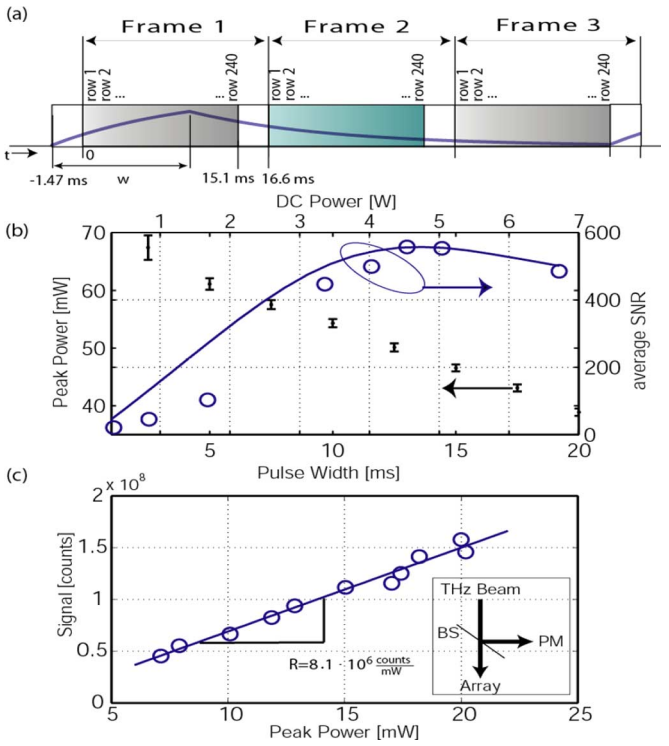

Fig. 2. (a) Solid trace shows signal/temperature time response to laser pulse of width w, over three frames. Frame is composed of sequential row samples of signal. Frames 1 and 3 are differenced to remove infrared background, leaving only THz signal. (b) Peak power and average SNR versus dc power dissipation/pulse width. Solid trace represents normalized calculated SNR, circles represent measured single-frame SNR averaged over focal plane (without lens), and dots with error bars represent THz laser power. (c) Total signal on focal-plane array versus peak power. Right inset shows experimental setup: THz beam is beam split (BS) into power meter (PM) and focal-plane array. (Color version available online at http://ieeexplore.ieee.org.)

by 20%∼40% by coating the surfaces with a thin sheet of polyethylene, which acts as an antireflection (AR) layer. The illuminated area in the object plane is roughly 3×3 cm, limited by the diameter of the first OAP. Also shown in Fig. 1 is the modified reflection mode setup, where a specular reflection is collected by the repositioned Si lens and camera.

The sampling sequence of the focal-plane array is shown in Fig. 2(a). Pixels in a row are sampled simultaneously with rows being acquired sequentially with a 64-μs period for each row until the last row (#240), after which there is 1.47 ms of inactive time. The focal plane is sampled at a 60-Hz frame rate (16.6 ms per frame).

The signal being sampled is modeled as the solid trace in Fig. 2(a) and results from a terahertz pulse, of width w, causing a temperature increase in the microbolometers. The pulse is applied at $t = -1.47$ ms and the signal rises with an ∼13-ms thermal time constant [12] until the end of the pulse, where the signal decays with the same time constant. Because the microbolometers are sensitive to both terahertz and infrared radiation, the uneven infrared background must be suppressed with either a long-wavelength-pass filter [10], which also attenuates the THz signal, or it can be subtracted using a reference frame, which has the additional benefit of reducing 1/f noise. The differencing scheme used here is described using Fig. 2(a): in frame 1, both terahertz and infrared background signals are present, and this frame is differenced with frame 3, where the terahertz signal has decayed sufficiently, resulting in cancellation of the common-mode infrared signal. The delay between the signal and reference is limited to one frame because longer delays introduce more 1/f and motion noise. A drawback of this scheme is the reduced frame rate of 20 Hz, but this rate is still sufficient for real-time imaging applications. To ensure that the observed differential signal was not due to thermal emission from the heated device at ∼5 W dc bias, we performed the same imaging measurements with the device operated above its maximum lasing temperature (∼70 K), and no differential signal was observed.

Fig. 2(b) shows the peak power P measured at the cryorefrigerator window using a thermopile power meter (ScienTech model AC2500H). The power decreases with pulsewidth due to active region heating in the QCL, which counteracts the benefit of the increased signal obtained with longer pulse widths. The pulsewidth is optimized for maximum differential signal by using the simple time constant model shown in Fig. 2(a), averaged over the focal plane. The optimum pulsewidth is ∼13.5 ms, corresponding to the highest measured SNR of ∼340 and ∼550 with and without the Si lens, respectively. We define SNR as the spatially and temporally averaged signal $\langle x \rangle$ divided by the RMS noise σ : $S/N = \langle x \rangle / \sigma$. Here, σ is taken in a 20-Hz (single frame) bandwidth with the terahertz beam blocked, characterizing only detector noise. While pulse-to-pulse stability does reduce SNR, it is seen as flickering, and the effect is mitigated by the preservation of relative values of adjacent pixels.

The optical NEP_O at 4.3 THz—the incident power at which SNR is unity—is obtained from the previous expression by normalizing σ to a 1-Hz bandwidth ($\sigma_{1\text{ Hz}} \sim 2.6$ counts$/\sqrt{\text{Hz}}$), and replacing $\langle x \rangle$ by the product of the NEP_O and a differential

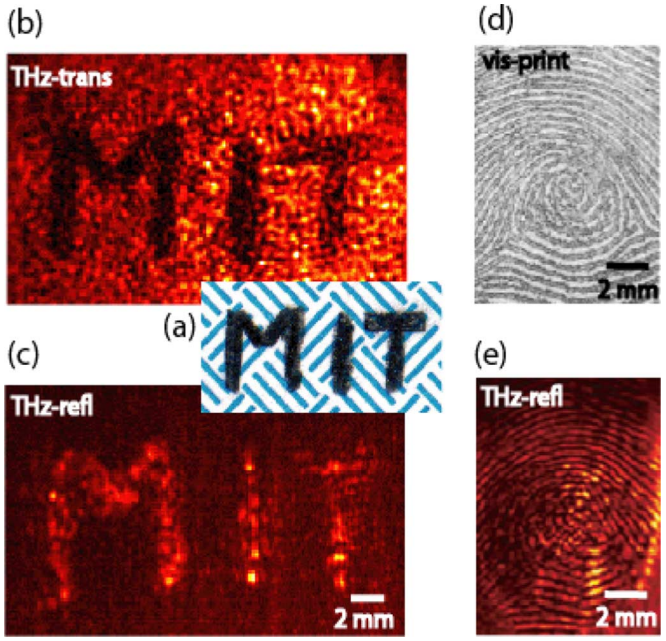

Fig. 3. Pencil letters written on inside of paper security envelope at visible frequencies. (a) Terahertz transmission mode, (b) one frame, and (c) terahertz reflection mode (20 frames). (d) Visible frequency thumb print and (e) terahertz reflection mode image of thumb of leading author (20 frames). (Color version available online at http://ieeexplore.ieee.org.)

responsivity R : $S/N = 1 = \langle x \rangle / \sigma_{1\ \mathrm{Hz}} = \mathrm{NEP}_O \cdot R/\sigma_{1\ \mathrm{Hz}}$. R is determined experimentally using the setup shown in the inset of Fig. 2(c) to measure the change of signal with respect to incident power—approximately 8.1×10^6 counts/mW. The incident power on the focal plane is measured using a beam splitter, which requires a low bias on the QCL for single-mode operation, as high biases cause multimode output, changing the beam-split ratio. The NEP_O is estimated to be $\sigma_{1\ \mathrm{Hz}}/R \sim 320\ \mathrm{pW}/\sqrt{\mathrm{Hz}}$ at 4.3-THz for this differential setup. This value is in reasonable agreement with a calculated value of $\sim 200\ \mathrm{pW}/\sqrt{\mathrm{Hz}}$ based on the electrical NEP_E of the microbolometers, modified for absorption/losses at the 70-μm wavelength and the differential scheme. At this long wavelength, absorption is estimated to be ∼4% using a transmission line model, and the transmission through the Ge window is estimated to be 38%, due to Fresnel losses and absorption. Frame subtraction increases the noise by a factor of $\sqrt{2}$, and the microbolometer thermal time constant limits their temperature rise to ∼42% of peak value.

The feasibility of a mail screening application is demonstrated by imaging the letters "MIT" written in pencil on the inside of a paper security envelope (∼14 dB loss at 4.3 THz), shown at visible frequencies in Fig. 3(a). A single terahertz differential frame, obtained in transmission mode, is shown in Fig. 3(b). The same image is shown in reflection mode in Fig. 3(c). In this image, a 20-frame average is shown due to the weaker reflected signal. Because the signal is the result of a specular reflection, the half of the envelope covering the lettering must be wedged slightly to prevent a strong reflection from the first surface. It should be pointed out that this particular imaging application cannot be done at other frequencies: X-rays lack contrast; millimeter-waves do not provide sufficient spatial resolution; and infrared radiation is heavily scattered and/or absorbed by fibrous materials [13]. A white-light image of an ink thumb print of the leading author is shown in Fig. 3(d), while the reflected terahertz 20-frame average image of the thumb flattened against a polyethylene wedge is shown in Fig. 3(e). The distance between the grooves in the print is $\sim 500\ \mu$m, demonstrating high-resolution capability.

While these still images are recognizable, when they are viewed in real time the integration of the eye and pattern recognition of the brain aid tremendously as seen in real-time video. Supplementary terahertz videos taken with the setup described in this letter are available at http://ieeexplore.ieee.org. These videos show transmission mode imaging of a plastic mechanical pencil, a metal screw embedded in polystyrene, and pencil lettering through and envelope. With additional QCLs the system will allow analytic real-time multifrequency imaging.

REFERENCES

[1] R. M. Woodward *et al.*, "Terahertz pulse imaging in reflection geometry of human skin cancer and skin tissue," *Phys. Med. Biol.*, vol. 47, no. 21, pp. 3853–3863, Oct. 2002.
[2] M. Nagel *et al.*, "Integrated THz technology for label-free genetic diagnostics," *Appl. Phys. Lett.*, vol. 80, no. 1, pp. 154–156, Jan. 2002.
[3] K. Kawase, "Terahertz imaging for drug detection and large-scale integrated circuit inspection," *Opt. Photon. News*, vol. 15, pp. 34–39, Oct. 2004.
[4] R. Köhler *et al.*, "Terahertz semiconductor-heterostructure laser," *Nature*, vol. 417, pp. 156–159, May 2002.
[5] M. Rochat *et al.*, "Low-threshold terahertz quantum-cascade lasers," *Appl. Phys. Lett.*, vol. 81, no. 8, pp. 1381–1383, Aug. 2002.
[6] B. S. Williams, H. Callebaut, S. Kumar, Q. Hu, and J. L. Reno, "3.4-THz quantum cascade laser based on longitudinal-optical-phonon scattering for depopulation," *Appl. Phys. Lett.*, vol. 82, no. 2, pp. 1015–1017, Feb. 2003.
[7] B. S. Williams, S. Kumar, Q. Hu, and J. L. Reno, "High-power terahertz quantum-cascade lasers," *Elec. Lett. Electron. Lett.*, vol. 42, no. 1, pp. 89–90, Jan. 2006.
[8] S. Kumar, B. S. Williams, Q. Hu, and J. L. Reno, "1.9-THz quantum-cascade lasers with one-well injector," *Appl. Phys. Lett.*, vol. 88, no. 3, p. 121123, Mar. 2006.
[9] J. Darmo *et al.*, "Imaging with a terahertz quantum cascade laser," *Opt. Expr.*, vol. 12, no. 9, pp. 1879–1884, May 2004.
[10] A. W. M. Lee and Q. Hu, "Real-time, continuous-wave terahertz imaging using a microbolometer focal-plane array," *Opt. Lett.*, vol. 30, no. 19, pp. 2563–2565, Oct. 2005.
[11] Q. Hu *et al.*, "Resonant-phonon-assisted THz quantum-cascade lasers with metal-metal waveguides," *Semiconduc. Sci. Technol.*, vol. 20, pp. S228–S236, 2005.
[12] N. Butler, R. Blackwell, R. Murphy, R. Silva, and C. Marshall, "Dual use, low cost microbolometer imaging system," in *Infrared Technology XXI, Proc. SPIE*, 1995, vol. 2552, pp. 583–592.
[13] J. E. Bjarnason, T. L. J. Chan, A. W. M. Lee, M. A. Celis, and E. R. Brown, "Millimeter-wave terahertz, and mid-infrared transmission through common clothing," *Appl. Phys. Lett.*, vol. 85, no. 4, pp. 519–521, Jul. 2004.